Dispersion characteristics of sound waves in a tunnel with an array of Helmholtz resonators

N. Sugimoto and T. Horioka
Department of Mechanical Engineering, Faculty of Engineering Science, University of Osaka, Toyonaka, Osaka 560, Japan

(Received 30 December 1993; accepted for publication 9 October 1994)

This paper examines dispersion characteristics of sound waves propagating in a tunnel with an array of Helmholtz resonators connected axially. Assuming plane waves over the tunnel's cross section except a thin boundary layer, weakly dissipative effects due to the wall friction and the thermoviscous diffusivity of sound are taken into account. Sound propagation in such a spatially periodic structure may be termed "acoustic Bloch waves." The dispersion relation derived exhibits peculiar characteristics marked by emergence of "stopping bands" in the frequency domain. The stopping bands inhibit selectively propagation of sound waves even if no dissipative effects are taken into account, and enhance the damping pronouncedly even in a dissipative case. The stopping bands result from the resonance with the resonators as side branches and also from the Bragg reflection by their periodic arrangements. In the "passing bands" outside of the stopping bands, the sound waves exhibit dispersion, though subjected intrinsically not only to the weak damping due to the dissipative effects but also to the weak dispersion due to the wall friction. Taking a plausible example, the dispersion relation and the Bloch wave functions for the pressure are displayed. Finally the validity of the continuum approximation for distribution of the Helmholtz resonators is discussed in terms of the dispersion relations.

PACS numbers: 43.20.Mv, 43.20.Hq, 43.20.Fn

INTRODUCTION

A tunnel with an array of Helmholtz resonators (called simply resonators hereafter) is promising for future high-speed trains such as magnetically levitated ones. For emergence of acoustic shock waves generated by traveling of trains is expected to be inhibited in this tunnel. The simplest architecture is such a tunnel that identical resonators are connected with equal axial spacing as shown in Fig. 1. The role of the array of resonators is to introduce dispersion as well as damping into nondispersive sound waves and especially to "disperse" pressure disturbances before shock formation. Its effectiveness is already demonstrated in the context of nonlinear acoustics based on the "continuum approximation" for axial distribution of the resonators.[1,2] This approximation is supported by the fact that the pressure disturbances leading to shock formation are propagated in the form of so-called infrasound. While the continuum approximation is therefore expected to hold in practical situations, this paper examines *linear* dispersion characteristics of sound waves over *all* frequency domain by taking full account of the discreteness in arrangements of the resonators. Among many modes of propagation in a tunnel as a waveguide, here we are concerned only with the plane-wave mode corresponding to the lowest mode.

By connecting the array of resonators, the tunnel has a spatially periodic structure. Wave propagation in a spatially periodic structure or field typified by the classical lattice[3] or the quantum field[4] is known as Bloch waves. They exhibit peculiar dispersion characteristics marked by emergence of "stopping bands" (or simply "stop bands") in a frequency domain. Such properties are expected to hold in the acoustics as well where the Bloch waves are not so familiar. Recently Bradley[5] has examined propagation of sound waves in a waveguide of rectangular duct loaded periodically with a quarter-wavelength tube and also confirmed their dispersion characteristics experimentally. This has motivated us to examine the Bloch waves in the tunnel with the array of Helmholtz resonators, which had already been proposed independently of Bradley's work, and also to check the validity of the continuum approximation employed previously.

The stopping bands are brought about physically by two mechanisms in the present problem. One is due to the resonance with the resonators as side branches when a frequency of sound waves coincides with its natural frequency. The side branch resonance then blocks forward transmission of sound wave. This is also the case when even a single resonator is connected to the tunnel. Another is due to the Bragg reflection when the axial spacing between the neighboring resonators becomes multiple of a half-wavelength of sound waves. In this sense, Bragg reflection is the very outcome of the periodic arrangement of the resonators.

Sound waves in the stopping bands are quickly damped spatially, in other words, become evanescent so that they cannot be propagated forward. The damping in this case has nothing to do with energy loss transformed into heat so it can occur in the lossless case. Frequency domains outside of the stopping bands are called "passing bands" (or simply "pass-bands") in which sound waves can be propagated without damping. Then the passing bands are characterized by emergence of dispersion due to the periodic arrangements of the resonators. In the lossy case, however, the sound waves are always subjected not only to the damping due to both the wall friction and the thermoviscous diffusive effect of sound,

 0001-4966/95/97(3)/1446/14/$6.00

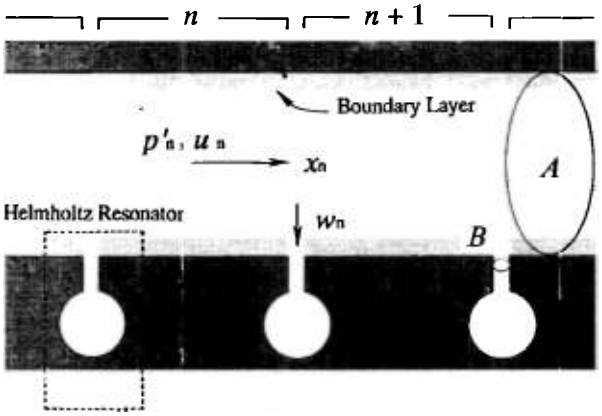

FIG. 1. A tunnel with an array of Helmholtz resonators. The tunnel is divided by the neighboring resonators into infinite number of intervals designated by n (=...−1,0,1,...) and the x_n axis in each interval is taken with its origin at the midpoint in the interval and along the axis of the tunnel x ($x_n=x-nd$).

but also to the weak dispersion due to the former effect. Therefore, the stopping bands and the passing bands cannot be distinguished sharply from each other unlike in the lossless case. But as far as the dissipative effects remain small, the stopping bands can be identified because the damping there is enhanced pronouncedly relative to the intrinsic damping.

In the following, we recapitulate the linear acoustic theory taking account of weakly dissipative effects. The dispersion relation is derived on assuming plane waves over a tunnel's cross section displaced by a thin boundary layer. The cross-sectional area of the resonators's throat is assumed to be so small that the resonators are regarded as being connected at "points" along the tunnel. By making use of the smallness of the resonator's volume relative to the tunnel's one per axial spacing, asymptotic behaviors of the stopping bands are examined and then the dispersion relation is solved numerically. For a plausible case, the dispersion relation and the Bloch wave functions for the pressure are displayed. Finally the validity of the continuum approximation is discussed in terms of the dispersion relation derived.

I. LINEAR ACOUSTIC THEORY

At the outset, we summarize results of the linear acoustic theory necessary to the analysis in the following sections. In the tunnel between the neighboring resonators, propagation of plane sound waves is assumed over the tunnel's cross section displaced by a thin boundary layer on the wall. This assumption is justified if the ratio of a typical thickness of the boundary layer $(\nu/\omega)^{1/2}$ to a hydraulic radius of the tunnel R is small enough:

$$\frac{(\nu/\omega)^{1/2}}{R}=\delta\ll 1, \tag{1}$$

where ν and ω denote, respectively, the kinematic viscosity of the air and an angular frequency. Although this ratio is found to be very small, the wall friction due to this thin boundary layer is taken into account. In addition, the diffusive effect of sound itself is also taken into account. Quantitatively, this effect is measured by the inverse of the acoustic Reynolds number Re defined by

$$\frac{\nu\omega}{a_0^2}=\frac{1}{\mathrm{Re}}\ll 1, \tag{2}$$

where a_0 is the sound speed. For a typical infrasound of frequency 5 Hz propagating in a tunnel of diameter 10 m say, δ is of order of 10^{-4}, while 1/Re is very small of order 10^{-8}! Hence the latter effect may be neglected.[6] For the sake of generality, however, the following formulation takes account of both effects only within the lowest order in expansion (often made implicitly) with respect to δ and 1/Re. But if 1/Re is comparable with δ^2, as is seen just above, the terms in 1/Re should be discarded or the quadratic terms in δ should necessarily be included so far as the first-order terms in 1/Re are retained.

Under these assumptions, sound propagation in the tunnel is governed by the following equation for the excess pressure p' over the atmospheric pressure p_0 (see the Appendix):

$$\frac{\partial^2 p'}{\partial t^2}-a_0^2\frac{\partial^2 p'}{\partial x^2}+\frac{2Ca_0^2\nu^{1/2}}{R}\frac{\partial^{-1/2}}{\partial t^{-1/2}}\left(\frac{\partial^2 p'}{\partial x^2}\right)-\nu_d\frac{\partial}{\partial t}\left(\frac{\partial^2 p'}{\partial x^2}\right)=0, \tag{3}$$

with $C=1+(\gamma-1)/\mathrm{Pr}^{1/2}$ and $\nu_d=\nu[4/3+\mu_v/\mu+(\gamma-1)/\mathrm{Pr}]$, where t and x are, respectively, the time and the spatial coordinate along the tunnel. With the Prandtl number Pr ($=\mu c_p/k_T$), μ, μ_v, c_p, and k_T denote, respectively, the coefficients of shear and bulk viscosities, the specific heat at constant pressure and the thermal conductivity, γ being the ratio of the specific heats. While the first two terms in Eq. (3) correspond to the well-known lossless wave equation, the third term represents the effect of the wall friction, which is given in the form of the hereditary integral known as the fractional derivative of the minus half-order with respect to t as follows:[7]

$$\frac{\partial^{-1/2}p'}{\partial t^{-1/2}}\equiv\frac{1}{\sqrt{\pi}}\int_{-\infty}^{t}\frac{1}{(t-t')^{1/2}}p(x,t')dt', \tag{4}$$

and the last term in Eq. (3) represents the diffusive effect, ν_d being the diffusivity of sound.

When a time-harmonic wave solution to p' is sought in the form of $\exp[i(kx-\omega t)]$, a wave number k is given in terms of an angular frequency ω (>0) as

$$k=\frac{\omega}{a_0}\left[1+\frac{(1+i)}{\sqrt{2}}\frac{C}{R}\left(\frac{\nu}{\omega}\right)^{1/2}+\frac{i\nu_d\omega}{2a_0^2}\right], \tag{5}$$

where the minus half-order derivative of the function $\exp(-i\omega t)$ is reduced to the Fresnel integrals and is evaluated simply to be $[(1+i)/\sqrt{2}]\exp(-i\omega t)=(-i\omega)^{-1/2}\times\exp(-i\omega t)$ as a formal extension of the ordinary rule of differentiation. Here note that $-k$ is also a solution for propagation toward the negative direction of x. With this excess pressure p', the axial velocity of the air u is similarly in the form of the time-harmonic wave p'/Z where Z is an acoustic impedance for the plane wave. Noting that the dis-

sipative effects are taken into account only within the lowest order in δ and 1/Re, Z is then given by

$$Z=\rho_0 a_0\left[1-\frac{(1+i)}{\sqrt{2}}\frac{C}{R}\left(\frac{\nu}{\omega}\right)^{1/2}+\frac{i\nu\omega}{2a_0^2}\left(\frac{4}{3}+\frac{\mu_v}{\mu}-\frac{\gamma-1}{\mathrm{Pr}}\right)\right]. \tag{6}$$

Next we consider the response of the resonator to pressure fluctuations at the orifice. The cavity's volume is much greater than the throat's one, so a motion of the air in the cavity is negligible. Hence we consider only the conservation of mass in the cavity:

$$V\frac{\partial\rho_c}{\partial t}=B\rho_0 w_c, \tag{7}$$

where V and ρ_c denote, respectively, the cavity's volume and the mean density of the air in it, while w_c denotes the velocity of the air flown into the cavity, averaged over the whole throat's cross section.

In the throat, the compressibility of the air is negligible because the throat's length L is much shorter than a typical wavelength a_0/ω (divided by 2π). Therefore the axial velocity w is regarded as being uniform along the throat so that w_c and w are set to be equal. Then integrating the linearized equation of motion along the throat's axis, it follows that

$$\rho_0 L\frac{\partial w}{\partial t}=-p_c'+p_t'-F_r, \tag{8}$$

where p_c' and p_t' represent, respectively, the excess pressure at the orifice on the cavity side and on the tunnel side and F_r designates the total friction on the throat wall, which is given by the hereditary integral as follows:[1]

$$F_r=\frac{2\rho_0 L\nu^{1/2}}{r}\left[\frac{1}{\sqrt{\pi}}\int_{-\infty}^{t}\frac{1}{(t-t')^{1/2}}\frac{\partial w(x,t')}{\partial t'}\,dt'\right]$$
$$=\frac{2\rho_0 L\nu^{1/2}}{r}\frac{\partial^{1/2}w}{\partial t^{1/2}}. \tag{9}$$

This integral takes the form derived by differentiating the derivative of minus half-order once with respect to t, so it is defined as the fractional derivative of half-order.

We now eliminate w $(=w_c)$ from Eqs. (7) and (8). By the adiabatic approximation for the air in the cavity, use is made of the relation $\partial\rho_c/\partial t=(d\rho_c/dp_c)\partial p_c/\partial t$, p_c being the mean pressure in the cavity. Furthermore approximating $dp_c/d\rho_c=a_0^2$, Eqs. (7) and (8) are combined into

$$\frac{\partial^2 p_c'}{\partial t^2}+\frac{2c_L\nu^{1/2}}{r}\frac{\partial^{3/2}p_c'}{\partial t^{3/2}}+\omega_0^2 p_c'=\omega_0^2 p_t', \tag{10}$$

where $p_c'(=p_c-p_0)$ is the excess pressure in the cavity and $\omega_0[=(Ba_0^2/LV)^{1/2}]$ is a natural frequency of the resonator. The derivative of three half-order is defined by differentiating the derivative of half-order once with respect to t. Here L is usually lengthened by the so-called end corrections and c_L is the correction factor for the viscous end correction.[1] But this factor is here considered to be incorporated into r formally by adjusting $r\to r/c_L$ and therefore c_L is set equal to unity in the following analysis.

For p_t' varying harmonically in the form of $P\times\exp(-i\omega t)$, the volume flow Bw from the tunnel into the throat is induced similarly in the form of $Q\exp(-i\omega t)$, where P and Q denote complex amplitudes. The ratio P/Q defines an acoustic impedance of the resonator Z_B depending on ω. By using Eqs. (7) to (9), Z_B is given as follows:

$$Z_B=\frac{p_e'}{Bw}=-\frac{i\rho_0 L}{B\omega}\left[\omega^2-\omega_0^2+\frac{\sqrt{2}(1+i)(\nu\omega^3)^{1/2}}{r}\right]. \tag{11}$$

II. DISPERSION RELATION

We now derive the dispersion relation of sound waves. Let the resonators be connected to an infinitely long tunnel with equal axial spacing d. Then the tunnel is separated into infinite number of intervals by neighboring resonators as shown in Fig. 1. Let each interval be numbered as n consecutively from minus to plus infinity ($n=\ldots,-1,0,1,\ldots$) and take the axial coordinate x along the tunnel with its origin at a midpoint in the interval $n=0$. The throat's cross-sectional area B is assumed to be so small compared with the tunnel's one A that the gap between the neighboring intervals may be negligible. In other words, the throats are regarded as being connected at "points" $x=(n+1/2)d$.

Let the excess pressure and the axial velocity in the interval n be denoted, with suffix n, by p_n' and u_n, respectively. Then p_n' is governed by Eq. (3) in the respective intervals. Assuming a time-harmonic disturbance in the form of $\exp(-i\omega t)$, p_n' is given by the superposition of two waves propagating toward the positive and negative directions of x as follows:

$$p_n'=f_n\exp[i(kx_n-\omega t)]+g_n\exp[i(-kx_n-\omega t)], \tag{12}$$

where k is a wave number given by the relation (5) and $x_n\equiv x-nd$ $(-d/2\leqslant x_n\leqslant d/2)$. Here f_n and g_n represent the respective complex wave amplitudes, which are to be determined by relations among the tunnels in the neighboring intervals and the resonator in between. Given the excess pressure (12), the axial velocity u_n in the interval n is derived immediately by using the acoustic impedance Z as follows:

$$u_n=\frac{f_n}{Z}\exp[i(kx_n-\omega t)]-\frac{g_n}{Z}\exp[i(-kx_n-\omega t)]. \tag{13}$$

At the connection point of the resonator $x=(n+1/2)d$, the boundary conditions require the continuity of mass flux

$$A\rho_0(u_n-u_{n+1})=B\rho_0 w_n, \tag{14}$$

and that of pressure

$$p_n'=p_{n+1}', \tag{15}$$

where w_n denotes the velocity of the air directed into the resonator from the tunnel.

By the continuity of the pressure, p_t' must be equal to p_n' and p_{n+1}'. Thus we can express w_n in terms of p_n' or p_{n+1}' by using the acoustic impedance Z_B. By the conditions

(14) and (15), the relation between (f_n, g_n) and (f_{n+1}, g_{n+1}) is then established through a transmission matrix $\mathbf{W}$ as follows:

$$\mathbf{X}_{n+1} = \mathbf{W}\mathbf{X}_n, \tag{16}$$

with

$$\mathbf{X}_n = \begin{bmatrix} f_n \\ g_n \end{bmatrix},$$

and

$$\mathbf{W} = \begin{bmatrix} (1 - 1/2\mathscr{R})\exp(ikd) & -1/2\mathscr{R} \\ 1/2\mathscr{R} & (1 + 1/2\mathscr{R})\exp(-ikd) \end{bmatrix}, \tag{17}$$

where $\mathscr{R} = Z_B/Z_A$ and $Z_A (= Z/A)$ is the acoustic impedance of the tunnel. Thus Eq. (16) can be solved successively, for example, if (f_0, g_0) is given.

But we consider an elementary solution to Eq. (16) in the form of $\mathbf{X}_n = \lambda^n \mathbf{C}$, where $\mathbf{C}$ is an arbitrary column vector. For this to be a solution, λ turns out to be eigenvalues of $\mathbf{W}$. When λ is set to be $\exp(iqd)$, q being allowed to be complex, q must satisfy the following dispersion relation so q is a complex-valued function of a real ω:

$$\cos(qd) = \cos(kd) - \frac{i}{2\mathscr{R}} \sin(kd), \tag{18}$$

where remember that k is given in terms of ω by (5). This dispersion relation is the same in form as that for a waveguide loaded periodically with a shunt impedance, though derivation here is different from Bradley's[5] and simple. Using the definitions of Z_A and Z_B, $i/2\mathscr{R}$ is expressed as follows:

$$\frac{i}{2\mathscr{R}} = -\frac{\kappa Z_1(\omega)}{2Z_2(\omega)} \equiv -\frac{\kappa \mathscr{Z}}{2}, \tag{19}$$

with

$$Z_1(\omega) = \frac{\omega d}{a_0}\left[1 - \frac{1+i}{\sqrt{2}}\frac{C}{R}\left(\frac{\nu}{\omega}\right)^{1/2} + \frac{i\nu\omega}{2a_0^2}\left(\frac{4}{3} + \frac{\mu_v}{\mu} - \frac{\gamma - 1}{\mathrm{Pr}}\right)\right], \tag{20}$$

and

$$Z_2(\omega) = \left(\frac{\omega}{\omega_0}\right)^2 - 1 + \frac{\sqrt{2}(1+i)}{r}\left(\frac{\nu}{\omega_0}\right)^{1/2}\left(\frac{\omega}{\omega_0}\right)^{3/2}. \tag{21}$$

Here $\kappa (= V/Ad)$ measures the smallness of the cavity's volume relative to the tunnel's one Ad per axial spacing. Unless the array of resonators were connected, i.e., $\kappa = 0$, q is reduced to k simply for the lossy propagation. Usually κ takes a small value compared to unity. Otherwise the resonators would be large unproportionally to the tunnel. As a plausible case, suppose a tunnel of diameter 10 m, to which a spherical cavity of diameter 6 m be connected through a throat of diameter 2 m and of length 3 m with axial spacing 10 m. Then κ takes the value 0.144.

Making use of the smallness of this parameter, Eq. (18) can be solved by expanding qd in terms of the power series in κ. Neglecting higher-order terms than the first order, it follows that

$$qd = kd - \kappa \mathscr{Z}/2 + O(\kappa^2). \tag{22}$$

Note that $-qd$ is also a solution to Eq. (18), which implies propagation toward the negative direction of x. With this understanding, only branches of qd having positive real part are concerned below. While k involves the intrinsic damping and dispersion due to the wall friction and the diffusive effect of sound itself, the second term on the right-hand side gives the additional ones, which are small quantities of $O(\kappa)$ so far as $\mathscr{Z}$ is of $O(1)$. But this approximate solution breaks down as $\mathscr{Z}$ diverges or becomes extremely large. It is further to be remarked that it also breaks down as $\sin(kd)$ vanishes or becomes extremely small.[8] In such exceptional cases, qd exhibits a peculiar behavior. We examine these cases in detail before seeking full numerical solutions.

A. Lossless case

For the sake of simplicity, at first, we consider a lossless case by neglecting the terms with ν. Then Eq. (18) is reduced to

$$\cos(qd) = \cos\psi + \frac{\kappa\psi \sin\psi}{2[(\omega/\omega_0)^2 - 1]}, \tag{23}$$

where ψ $(= \omega d/a_0)$ is the ratio of the axial distance d to a typical wavelength a_0/ω.

Denoting the right-hand side of Eq. (23) by ξ, types of root qd are classified according as $|\xi| \leq 1$, $\xi > 1$ or $\xi < -1$. For $|\xi| \leq 1$, qd is given simply by $\pm\cos^{-1}\xi$. If $\cos^{-1}\xi$ is defined to be the principal value between zero and π, qd is allowed to have additive arbitrariness $\pm 2\pi j$ $(j = 1,2,3,\ldots)$. Of course, q is always accompanied with this arbitrariness not only for $|\xi| \leq 1$ but also for all values of ξ. But λ $[= \exp(iqd)]$ is uniquely determined as $\lambda = \xi \pm i(1 - \xi^2)^{1/2}$. If $|\xi| > 1$, qd becomes complex. For $\xi > 1$, $qd = \pm i \cosh^{-1}\xi$ where $\cosh^{-1}\xi$ is defined to be positive by taking $\log[\xi + (\xi^2 - 1)^{1/2}]$, while for $\xi < -1$, $qd = \pi \pm i \cosh^{-1}|\xi|$. In either case, the product of the two roots of $\lambda [= \xi \pm (\xi^2 - 1)^{1/2}]$, both being real, is unity so that the roots are reciprocal. For $|\xi| \leq 1$, on the other hand, note that they are complex conjugate with each other.

To check whether or not $|\cos(qd)|$ is greater than unity, it is convenient to rewrite Eq. (23) in the following two expressions:

$$\cos(qd) - 1 = -\sin^2\left(\frac{\psi}{2}\right)\left[2 - \frac{\kappa\psi}{(\omega/\omega_0)^2 - 1}\cot\left(\frac{\psi}{2}\right)\right], \tag{24}$$

$$-1 - \cos(qd) = -\cos^2\left(\frac{\psi}{2}\right)\left[2 + \frac{\kappa\psi}{(\omega/\omega_0)^2 - 1}\tan\left(\frac{\psi}{2}\right)\right]. \tag{25}$$

If either one or both of the right-hand sides of Eqs. (24) and (25) is positive, qd is no longer real but complex. For this to be so, there are two cases. One occurs as $\omega \to \omega_0$, while the other occurs as $\tan(\psi/2)$ or $\cot(\psi/2)$ diverges, i.e., $\sin\psi \to 0$.

The former corresponds to the side branch resonance when a frequency of sound wave coincides with the natural frequency of the resonator. The latter occurs when $\omega d/a_0$ becomes $m\pi$ ($m=1,2,3,\ldots$), i.e., the axial spacing d becomes multiple of a half-wavelength $\pi a_0/\omega$. This is a Bragg reflection by the periodic arrangements of the resonators. When the imaginary part of q exists, the wave grows or decays spatially because the solutions q to Eq. (23) appear evidently in the complex conjugate pair. But only the branch for the decay should be chosen in the present context since no energy sources exist in the problem. Hence the stopping band appears in the frequency.

Let us first consider the stopping band near $\omega=\omega_0$. Making use of the small parameter κ, the asymptotic behavior as $\omega\to\omega_0$ is examined by setting $\omega/\omega_0=1+\Delta$. Here $|\Delta|$ is assumed to be small enough relative to unity. Then ψ is also set as $\psi/\psi_0=1+\Delta$ with $\psi_0=\omega_0 d/a_0$. From the relations (24) and (25), it is found that ξ takes unity, within the first order of Δ, at $\Delta=\Delta_+$ given by

$$\Delta_+=\frac{\kappa\psi_0}{4}\cot\left(\frac{\psi_0}{2}\right), \tag{26}$$

while ξ takes minus unity at $\Delta=\Delta_-$ given by

$$\Delta_-=-\frac{\kappa\psi_0}{4}\tan\left(\frac{\psi_0}{2}\right). \tag{27}$$

Hence the stopping band appears in the range $1+\Delta_-<\omega/\omega_0<1+\Delta_+$ if $\tan(\psi_0/2)>0$ or $1+\Delta_+<\omega/\omega_0<1+\Delta_-$ if $\tan(\psi_0/2)<0$. The width of the stopping band is found to be small of order κ. As ω approaches ω_0, Eq. (23) is asymptotically given by

$$\cos(qd)=\frac{\kappa\psi_0\sin\psi_0}{4\Delta}+O(1). \tag{28}$$

As $\Delta\to 0$, the imaginary part of qd diverges as $\log|\kappa\psi_0\sin\psi_0/2\Delta|$. But if $\sin\psi_0>0$, then its real part is fixed at π for $\Delta<0$, i.e., $\omega/\omega_0<1$ while zero for $\Delta>0$, i.e., $\omega/\omega_0>1$. Conversely if $\sin\psi_0<0$, the real part is zero for $\omega/\omega_0<1$ while π for $\omega/\omega_0>1$. Here it is interesting to examine a special case in which $\tan(\psi_0/2)$ or $\cot(\psi_0/2)$ diverges, i.e., $\omega_0 d/a_0$ becomes multiple of π. This is the case when the natural frequency of the resonator happens to coincide with that for the Bragg reflection. Before going into this case in detail, we examine the stopping bands near $\omega=m\pi a_0/d=\omega_m$ ($m=1,2,3,\ldots$).

In this case, we set $\omega/\omega_m=1+\Delta$ ($|\Delta|\ll 1$) so that $\psi/\psi_m=1+\Delta$ with $\psi_m=m\pi$. Then Eq. (23) is approximately given as

$$\cos(qd)=(-1)^m(1+\Xi)+O(\kappa\Delta^2), \tag{29}$$

where

$$\Xi=-\frac{(m\pi)^2}{2}(\Delta-\Delta_m)\Delta\leqslant\frac{(m\pi\Delta_m)^2}{8}, \tag{30}$$

with

$$\Delta_m=\frac{\kappa}{(\omega_m/\omega_0)^2-1}. \tag{31}$$

The stopping band appears for $\Xi>0$, i.e., $1<\omega/\omega_m<1+\Delta_m$ if $\Delta_m>0$, while $1+\Delta_m<\omega/\omega_m<1$ if $\Delta_m<0$. Depending on the sign of Δ_m, the stopping band appears either side of $m\pi$ only and its width is small of order κ. The magnitude of the imaginary part of qd is given by $(2\Xi)^{1/2}$ for $\Xi>0$. Thus it is bounded, unlike the side branch resonance, with its maximum given by $m\pi|\Delta_m|/2$ at $\Delta=\Delta_m/2$. As m increases, the width of the stopping band becomes narrower as $1/m^2$ and the maximum value of the imaginary part becomes smaller as $1/m$. On the other hand, the real part of qd is fixed at zero or π according as m is even or odd, respectively. If the additive arbitrariness is employed suitably, the real part may be taken as $m\pi$.

Here we return to the special case in which ω_0 is equal to one of the ω_m's. Then Ξ in (29) is modified into

$$\Xi=-\frac{(m\pi)^2}{2}\left(\Delta^2-\frac{\kappa}{2}\right)+O(\kappa\Delta). \tag{32}$$

Therefore the stopping band appears in the region $1-(\kappa/2)^{1/2}<\omega/\omega_0<1+(\kappa/2)^{1/2}$, which is widened to be of order $\sqrt{\kappa}$. The imaginary part of qd is given by $(2\Xi)^{1/2}$ only for $\Xi>0$. Thus it is found to be bounded to attain the maximum $(\kappa/2)^{1/2}m\pi$ at $\Delta=0$. The real part of qd is then fixed at $m\pi$.

B. Lossy case

Let us next look at the dissipative effect by reviving the terms with ν. In this case, qd is always complex, as the solution (22) shows, so that the stopping bands are not distinguished clearly from the passing bands. Even so, the stopping bands appear prominently as far as the dissipative effects are small.

The side branch resonance in this case takes place at a frequency slightly down from ω_0 to $\omega_{0\nu}$ given by

$$\omega_{0\nu}=\omega_0\left[1-\frac{1}{\sqrt{2}r}\left(\frac{\nu}{\omega_0}\right)^{1/2}\right], \tag{33}$$

where the quadratic terms in $(\nu/\omega_0)^{1/2}/r$ have been neglected. Here we set $\omega/\omega_{0\nu}=1+\Delta$ ($|\Delta|\ll 1$) so that $\psi/\psi_{0\nu}=1+\Delta$ with $\psi_{0\nu}=\omega_{0\nu}d/a_0$. Equation (18) is approximated to be

$$\cos(qd)=\frac{\kappa\psi_0\sin\psi_0}{4(\Delta+i\sigma)}+O(1)\quad\text{with}\quad\sigma=\frac{(\nu/\omega_0)^{1/2}}{\sqrt{2}r}. \tag{34}$$

Separating q into the real and imaginary parts by setting $q=q_r+iq_i$, the imaginary part q_i in the stopping band is given as follows:

$$q_i d=\log\left(\frac{\kappa\psi_0|\sin\psi_0|}{2(\Delta^2+\sigma^2)^{1/2}}\right). \tag{35}$$

Due to a small but finite value of σ, $q_i d$ becomes bounded and takes the maximum value

$$\max(q_i d)=\log\left(\frac{\kappa\psi_0|\sin\psi_0|}{2\sigma}\right) \tag{36}$$

at $\Delta=0$. A half of the maximum value is taken at

$$\Delta=\pm\left(\frac{\kappa\sigma\psi_0|\sin\psi_0|}{2}-\sigma^2\right)^{1/2}. \tag{37}$$

On the other hand, the real part q_r is given by

$$q_r d=\begin{cases}\tan^{-1}(\sigma/\Delta), & \text{if } \sin\psi_0>0,\\ \tan^{-1}(\sigma/\Delta)+\pi, & \text{if } \sin\psi_0<0,\end{cases} \tag{38}$$

where $\tan^{-1}(\sigma/\Delta)$ is defined by taking the principal value between zero and π. With this definition, $q_r d$ changes smoothly across $\Delta=0$. If $\sin\psi_0>0$ and $\sigma\ll|\Delta|$, $q_r d$ takes π for $\Delta<0$, while it takes zero for $\Delta>0$. If $\sin(\psi_0)<0$, $q_r d$ takes 2π for $\Delta<0$, while it takes π for $\Delta>0$. On identifying 2π to be zero, the result is consistent with that in the lossless case.

Next we consider the stopping bands due to the Bragg reflection. For the real part of $\sin(kd)$ to vanish, a frequency is shifted from ω_m slightly down by the wall friction. Such frequencies $\omega_{m\nu}$ $(m=1,2,3,\ldots)$ are evaluated as

$$\omega_{m\nu}=\omega_m\left[1-\frac{C}{\sqrt{2R}}\left(\frac{\nu}{\omega_m}\right)^{1/2}\right]. \tag{39}$$

By the usual procedure, we set ω and ψ as follows: $\omega/\omega_{m\nu}=\psi/\psi_{m\nu}=1+\Delta$ $(|\Delta|\ll1)$ with $\psi_{m\nu}=\omega_{m\nu}d/a_0$. For convenience, we also introduce $\tilde{\Delta}$ through the relation

$$\frac{\omega d}{a_0}\left[1+\frac{C}{\sqrt{2R}}\left(\frac{\nu}{\omega}\right)^{1/2}\right]=m\pi(1+\tilde{\Delta}). \tag{40}$$

Then Δ and $\tilde{\Delta}$ are related, correctly up to $O(\delta)$, by

$$\tilde{\Delta}=\left[1+\frac{C}{2\sqrt{2R}}\left(\frac{\nu}{\omega_m}\right)^{1/2}\right]\Delta. \tag{41}$$

Using $\tilde{\Delta}$, it follows from Eq. (18) that

$$\cos(qd)=(-1)^m(1+\Xi)+O(\kappa\delta\tilde{\Delta},\kappa\tilde{\Delta}/\mathrm{Re},\kappa\tilde{\Delta}^2,\delta\tilde{\Delta}^2,\tilde{\Delta}^2/\mathrm{Re}), \tag{42}$$

with

$$\Xi=-i(m\pi)^2\nu_m\left(\tilde{\Delta}-\frac{\Delta_m}{2}\right)-\frac{(m\pi)^2}{2}(\tilde{\Delta}-\Delta_m)\tilde{\Delta}, \tag{43}$$

and

$$\nu_m=\frac{C}{\sqrt{2R}}\left(\frac{\nu}{\omega_m}\right)^{1/2}+\frac{\nu_d\omega_m}{2a_0^2}. \tag{44}$$

Letting $qd=m\pi+\rho_r+i\rho_i$, we have

$$\rho_i=\frac{m\pi}{\sqrt{2}}\left\{\frac{\Delta_m^2}{4}-\phi^2+\left[\left(\frac{\Delta_m^2}{4}-\phi^2\right)^2+4\nu_m^2\phi^2\right]^{1/2}\right\}^{1/2}, \tag{45}$$

where $\phi=\tilde{\Delta}-\Delta_m/2$. It can be easily verified that ρ_i has a single and symmetric peak at $\phi=0$. Its maximum is given by the same value $m\pi|\Delta_m|/2$ as in the lossless case and its half value is taken at

$$\tilde{\Delta}=\pm\frac{\sqrt{3}\Delta_m^2}{4(\Delta_m^2-16\nu_m^2)^{1/2}}. \tag{46}$$

While this width should be corrected in Δ slightly by the relation (41), it is almost given by $\sqrt{3}\Delta_m/4$ because $\nu_m\ll|\Delta_m|$ so that the width is found to be of order κ. As $|\Delta|$ becomes large, ρ_i tends to $m\pi\nu_m$, which corresponds to the imaginary part of kd in (22). With the imaginary part ρ_i thus obtained, the real part ρ_r is derived as

$$\rho_r=\frac{(m\pi)^2\nu_m}{\rho_i}\left(\tilde{\Delta}-\frac{\Delta_m}{2}\right), \tag{47}$$

and ρ_r changes antisymmetrically with respect to $\tilde{\Delta}=\Delta_m/2$.

Finally we examine a special case in which a frequency for the side branch resonance coincides with one of the frequencies for the Bragg reflection, i.e., $\omega_{0\nu}=\omega_{m\nu}$, where m is fixed to be a certain integer. For this to be so, ω_0 and ω_m must satisfy the relation:

$$\omega_0=\omega_m\left[1+\frac{1}{\sqrt{2}}\left(\frac{1}{r}-\frac{C}{R}\right)\left(\frac{\nu}{\omega_m}\right)^{1/2}\right]. \tag{48}$$

We set $\omega/\omega_{0\nu}=\psi/\psi_{0\nu}=1+\Delta$ $(|\Delta|\ll1)$. Substituting this into Eq. (18) and keeping the lowest terms in Δ, it is approximated as

$$\cos(qd)=(-1)^m\left[1+\frac{\kappa(m\pi)^2}{4}\left(\frac{\Delta+i\nu_m}{\Delta+i\sigma}\right)\right]+O(\kappa\Delta,\kappa\delta,\kappa/\mathrm{Re}), \tag{49}$$

where $\nu_m\ll\sigma$. When qd is separated into the real and imaginary parts by setting $qd=m\pi+\rho_r+i\rho_i$, it is found by the straightforward calculations that

$$\rho_i=\frac{\sqrt{\kappa}m\pi}{2}\left[\frac{\Delta^2+\sigma\nu_m}{\Delta^2+\sigma^2}+\left(\frac{\Delta^2+\nu_m^2}{\Delta^2+\sigma^2}\right)^{1/2}\right]^{1/2}. \tag{50}$$

It is found that ρ_i is symmetric with respect to $\Delta=0$. It decreases monotonically from $(\kappa/2)^{1/2}m\pi$ at both infinity of Δ toward $(\kappa/2)^{1/2}m\pi(\nu_m/\sigma)^{1/2}$ at $\Delta=0$. The asymptotic value for a large value of $|\Delta|$ agrees with the maximum in the lossless case when the side branch resonance and the Bragg reflection overlap. Since $\nu_m/\sigma\ll1$, interestingly enough, the dissipative effect is found to decrease ρ_i significantly near $\Delta=0$. On the other hand, the real part q_r is given by

$$\rho_r=\frac{\kappa(m\pi)^2(\sigma-\nu_m)\Delta}{4(\Delta^2+\sigma^2)\rho_i}. \tag{51}$$

Because of the function $\Delta/(\Delta^2+\sigma^2)$, ρ_r becomes antisymmetric with respect to $\Delta=0$ and tends to vanish as $|\Delta|$ increases.

C. Numerical results

Let us show graphically the dispersion relation between ω and q by solving Eq. (18) numerically. For an air at 15 °C, the following data are used: $a_0=340$ m/s, $\gamma=1.40$, $\mathrm{Pr}=0.72$, $C=1.47$, $\mu_v/\mu=0.60$, $\nu=1.45\times10^{-5}$ m^2/s, and $\nu_d=2.49\nu$. Supposing that the resonator already specified is connected to the tunnel of diameter 10 m with the axial spacing 10 m, it follows that $V=36\pi$ m^3, $A=25\pi$ m^2, $d=10$ m, $r=1$ m, $B=\pi$ m^2, $L=3$ m, and $\kappa=0.144$. The natural frequency ω_0 is then 5.2 Hz and the frequency ω_1 for the Bragg reflection with $m=1$ is 17 Hz. The frequency for the higher Bragg reflection with $m\geq2$ is simply $m\omega_1$. From these data, it is found that $(\nu/\omega_0)^{1/2}/R=1.3\times10^{-4}$ and $\nu_d\omega_0/a_0^2=1.0\times10^{-8}$. If a 1/200-scale model is considered,

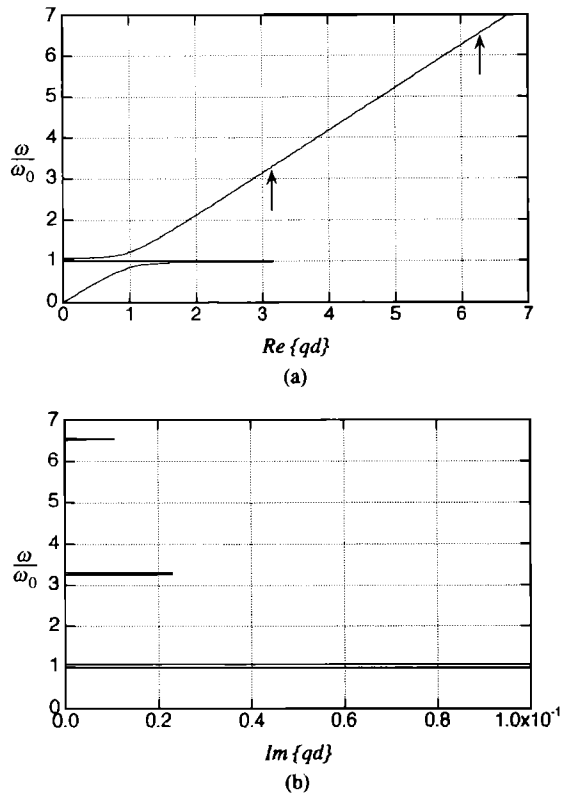

FIG. 2. Dispersion relation of sound waves in the lossless case. (a) and (b) show, respectively, the real and imaginary parts of qd as the abscissa and the normalized frequency ω/ω_0 as the ordinate where the two arrows in (a) indicate the real parts fixed at π and 2π for the Bragg reflections and the imaginary part vanishes outside of the stopping band.

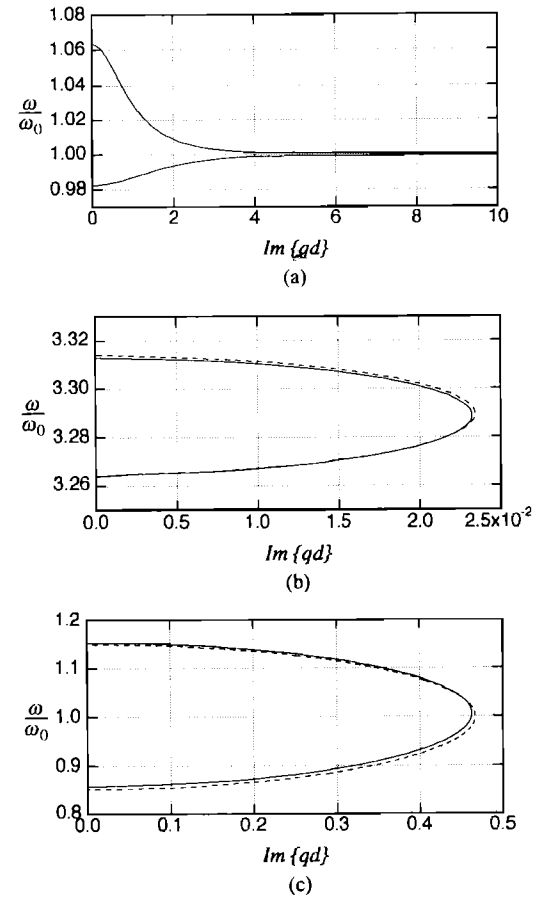

FIG. 3. Local structure of the stopping bands. (a), (b), and (c) show, respectively, the imaginary parts due to the side branch resonance, due to the Bragg reflection with $m=1$ and in the degenerate case of the side branch resonance and the Bragg reflection with $m=1$ where the axial spacing is changed from $d=10$ m to $d=32.65$ m. The solid and broken lines represent, respectively, the numerical solutions and the approximate solutions $(2\Xi)^{1/2}$ with (30) in (b) and (32) in (c).

they still take such small values as $(\nu/\omega_0)^{1/2}/R=1.9\times10^{-3}$ and $\nu_d\omega_0/a_0^2=2.0\times10^{-6}$ for $\omega_0=1.04$ kHz. Because 1/Re is comparable with δ^2, we retain only terms in δ and ignore those in 1/Re.

Figure 2 exhibits the global features of the dispersion relation in the lossless case. Figure 2(a) and (b) show, respectively, the real and imaginary parts of qd as the abscissa and the normalized frequency ω/ω_0 as the ordinate. Here only the branches with the positive real part are drawn so that they may become continuous at $qd=\pi,2\pi,\ldots$ and nondecreasing as ω increases across there by using the additive arbitrariness $\pm2\pi j$ $(j=1,2,3,\ldots)$. But they may be discontinuous and/or decreasing in principle. It is noted that the full dispersion relation is given by an infinite number of branches consisting of the fundamental branch qd now being obtained together with $-qd$ and those differing by $\pm2\pi j$. Two arrows in Fig. 2(a) indicate the real parts fixed at π and 2π during the Bragg reflections with $m=1$ and $m=2$, respectively $(\omega_1/\omega_0=3.265$ and $\omega_2/\omega_0=6.530)$. Figure 2(b) shows that the imaginary part appears only in the narrow regions over the frequency domain, which constitutes the stopping bands. Here the imaginary part due to the side branch resonance diverges as $\omega/\omega_0\to1$.

The local structures of the respective stopping bands are enlarged in Fig. 3. Figure 3(a) shows the stopping band for ω/ω_0 between 0.983 and 1.064. The band width agrees very well with (26) and (27) derived asymptotically $(1+\Delta_-=0.982$ and $1+\Delta_+=1.066)$. Figure 3(b) shows the stopping band due to the Bragg reflection with $m=1$. Here and hereafter the solid line represents the numerical solutions while the broken line represents the approximate solutions, unless otherwise stated. The broken line in this figure is drawn according to $(2\Xi)^{1/2}$ with (30). The stopping band appears for ω/ω_0 between 3.265 and 3.313 and the maximum value of the imaginary part is 2.32×10^{-2}. These numerical values are to be compared with the approximate ones, i.e., the lower and upper bounds of the stopping band are given by 3.265 and 3.314 while the maximum value is given by 2.34×10^{-2}. Figure 3(c) shows the stopping band in the degenerate case in which the side branch resonance coincides with the Bragg reflection with $m=1$. This case occurs when the axial spacing is changed from $d=10$ m to $d=32.65$ m (so that $\kappa=4.41\times10^{-2}$). The structure of the side branch resonance seen in Fig. 2 is destroyed and the one of the Bragg reflection prevails instead. The stopping band is now widened for ω/ω_0 between 0.859 and 1.152 in spite of the smaller value of κ compared with the case in Fig. 3(a). The approximate lower and upper bounds of the stopping bands are given by 0.852 and 1.149. The imaginary part takes the maximum value 0.4627 at a frequency slightly shifted above

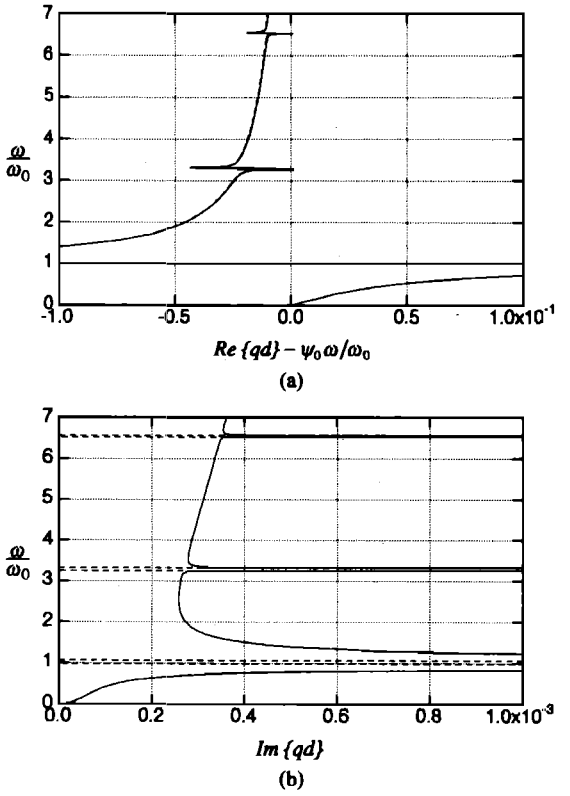

FIG. 4. Dispersion relation of sound waves in the lossy case. (a) and (b) show, respectively, the real part of qd minus $\psi_0\omega/\omega_0$ with $\psi_0=\omega_0 d/a_0$ and the imaginary part of qd as the abscissa and the normalized frequency ω/ω_0 as the ordinate where the solid line represents the numerical solutions in the lossy case while the broken line represents the numerical ones in the lossless case for reference and the horizontal scale in (b) is magnified by 10^3 times that in Fig. 2.

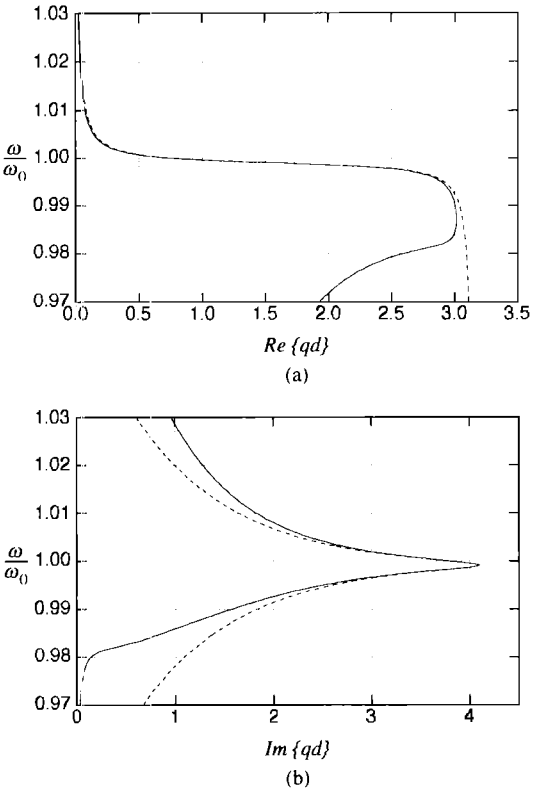

FIG. 5. Local structure of the stopping band due to the side branch resonance in the lossy case. (a) and (b) show, respectively, the real and imaginary parts of qd as the abscissa and the normalized frequency ω/ω_0 as the ordinate where the solid lines represent the numerical solutions while the broken line represent the approximate solutions (35) and (38).

to $\omega/\omega_0=1.005$, which is to be compared with the approximate result 0.4665 at $\omega/\omega_0=1$.

Next we take account of the dissipative effects. If the dispersion relation is displayed with the same scalings as in Fig. 2, no differences can be recognized except that the imaginary part due to the side branch resonance is now suppressed to be finite. In order to make the differences stand out, a kind of deviations from the dispersion relation in the lossless case is illustrated. In the lossless case, q approaches ω/a_0 as ω increases. This means that the sound waves tend to be nondispersive in the high-frequency limit just as in the tunnel without the array of resonators. In view of this, it appears to be informative to illustrate the real part of qd subtracted by $\omega d/a_0$. Figure 4(a) shows the real part $qd-\psi_0\omega/\omega_0$ with $\psi_0=\omega_0 d/a_0$ as the abscissa and the normalized frequency ω/ω_0 as the ordinate. The solid line represents the numerical solutions in the lossy case while the broken line represents the numerical ones in the lossless case. Even in this figure, the dissipative effects are found to be very small. In Fig. 4(a), the real part is of course bounded as $\omega/\omega_0\to 1$. The real part for the Bragg reflections is seen to exhibit a structure similar to that of the side branch resonance where the real part qd minus $\psi_0\omega/\omega_0$ vanishes at $\omega=\omega_m$ in the lossless case. On the other hand, Fig. 4(b) shows the imaginary part of qd with the abscissa magnified by 10^3 times compared with that in Fig. 2. The imaginary part is always present over all frequency domain but it is enhanced pronouncedly due to the side branch resonance and the Bragg reflections. As ω increases, the imaginary part due to the intrinsic damping is seen to increase.

The subsequent figures, Figs. 5 and 6, show the local structures of the respective stopping bands due to the side branch resonance and the Bragg reflection with $m=1$. In Fig. 5, the broken lines represent the approximate solutions (35) and (38). It is seen that they can describe very well a sharp transition behavior in the vicinity of $\omega/\omega_0=1$. The frequency for the peak in the imaginary part is lowered slightly to $\omega_0/\omega_0=0.999$ according to (33). The maximum value 4.102 and its half-width 0.01457 agree well with the approximate values 4.101 and 0.01450 calculated by (36) and (37), respectively. In Fig. 6, the broken lines represent the approximate solutions (45) and (47). The imaginary part attains the maximum value 2.319×10^{-2} at $\omega/\omega_0=3.289$, which provide good agreement with the approximate one 2.342×10^{-2} at $\omega/\omega_0=3.287$. The half-width 0.04138 is to be compared with the approximate one 0.04214 based on (46). Finally the global features of the dispersion relation in the degenerate case corresponding to Fig. 3(c) is depicted in Fig. 7. Two arrows indicate the real parts for the Bragg reflections with $m=2$ and $m=3$. The very sharp drop in the imaginary part near $\omega/\omega_0=1$ is observed. Its local structure is shown in Fig. 8 with the broken lines given by (50) and (51). The minimum value 0.1787 agrees well with the approximate one 0.1788.

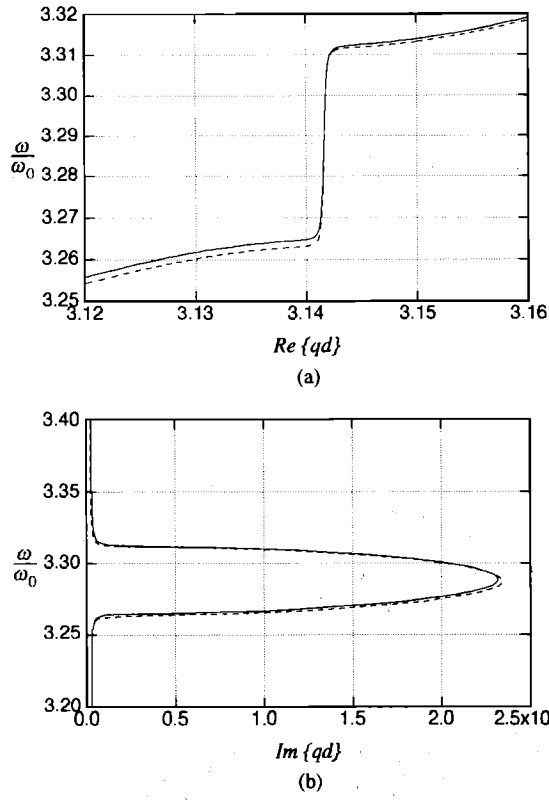

FIG. 6. Local structure of the stopping band due to the Bragg reflection with $m=1$ in the lossy case. (a) and (b) show, respectively, the real and imaginary parts of qd as the abscissa and the normalized frequency ω/ω_0 as the ordinate where the solid lines represent the numerical solutions while the broken line represent the approximate solutions (45) and (47).

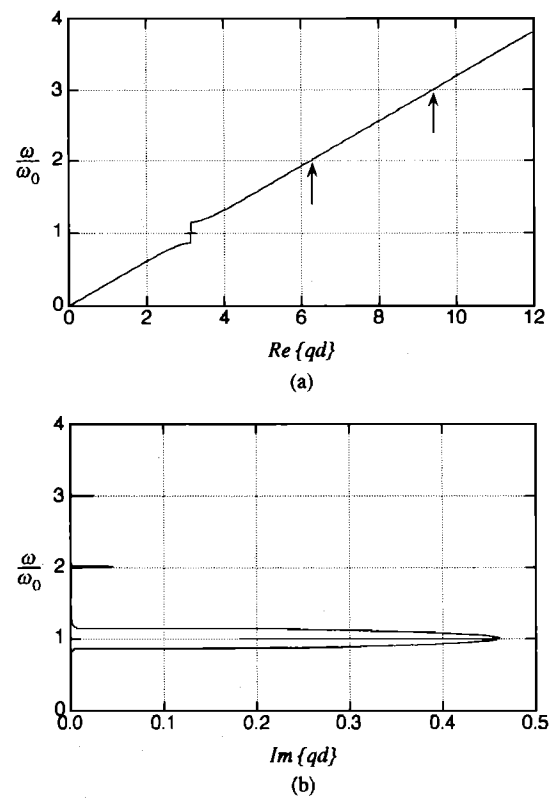

FIG. 7. Dispersion relation of sound waves in the lossy and degenerate case of the side branch resonance and the Bragg reflection with $m=1$ for the axial spacing $d=32.65$ m. (a) and (b) show, respectively, the real and imaginary parts of qd as the abscissa and the normalized frequency ω/ω_0 as the ordinate where the two arrows in (a) indicate the real parts for the Bragg reflections and the solid line along $\omega/\omega_0=1$ in (b) shows the sharp drop of the imaginary part from its peak.

III. BLOCH WAVE FUNCTIONS

Since the relation between ω and q (i.e., λ) is now available, we can specify the pressure field p'_n given by (12). For the respective eigenvalues $\lambda^{\pm}$, the eigenvectors of the matrix $\mathbf{W}$ are denoted by $\mathbf{C}^{\pm}$, respectively. Here and hereafter the sign "$\pm$" is understood to be ordered vertically and λ^+ and λ^- are defined to correspond, respectively, to propagation toward the positive and negative direction of x. A general solution $\mathbf{X}_n$ to Eq. (16) is then represented by the superposition of the two eigenvectors:

$$\mathbf{X}_n=(\lambda^+)^n\mathbf{C}^+ +(\lambda^-)^n\mathbf{C}^-. \tag{52}$$

Denoting $\mathbf{C}^{\pm}$ by the components $(c_1^{\pm},c_2^{\pm})^T$, T being the transposition, and setting $\lambda^{\pm}=\exp(\pm iqd)$ where the real part of q is chosen positive, p'_n is expressed as follows:

$$\begin{aligned} p'_n &= [c_1^+ \exp(ikx_n)+c_2^+ \exp(-ikx_n)]\exp[i(qnd-\omega t)] \\ &\quad +[c_1^- \exp(ikx_n)+c_2^- \exp(-ikx_n)]\exp[i(-qnd-\omega t)]. \end{aligned} \tag{53}$$

Here we introduce the functions $\Phi^{\pm}(x_n)$:

$$\Phi^{\pm}(x_n)=[c_1^{\pm} \exp(ikx_n)+c_2^{\pm} \exp(-ikx_n)] \exp(\mp iqx_n), \tag{54}$$

where $\Phi^{\pm}(x_n)$ are defined only for $-d/2\leqslant x_n\leqslant d/2$ and $\Phi^{\pm}(x_n)$ takes the same values at both ends $x_n=\pm d/2$ due to the boundary condition (15). We then extend $\Phi^{\pm}(x_n)$ periodically into the outside of the interval of definition with period d. Denoting the functions by $\Phi^{\pm}(x)$ $[=\Phi^{\pm}(x+d)]$, p' at an arbitrary point of x can be expressed, with the suffix n dropped, in the form of

$$p'=\Phi^+(x)\exp[i(qx-\omega t)]+\Phi^-(x)\exp[i(-qx-\omega t)]. \tag{55}$$

The first and second terms represent the waves propagating toward the positive and negative directions of x, respectively. If q is real, i.e., ω is chosen within the passing bands in the lossless case, the exponential functions are periodic with period $2\pi/q$. This period is usually incommensurate with the period d of $\Phi^{\pm}$, so the product of both functions no longer become periodic but aperiodic. Note that even if temporally monochromatic, it is not so spatially. Each of the solutions $\Phi^{\pm}(x)\exp[i(\pm qx-\omega t)]$ is called a "Bloch wave function," while q is called a "Bloch wave number."

The functions $\Phi^{\pm}(x)$ can be determined except for scale factors because only the ratios $c_2^{\pm}/c_1^{\pm}$ are specified as

$$\frac{c_2^{\pm}}{c_1^{\pm}}=-\frac{2}{\kappa\mathscr{Z}}\left[\pm\sin(qd)-\sin(kd)+\frac{\kappa\mathscr{Z}}{2}\cos(kd)\right], \tag{56}$$

or

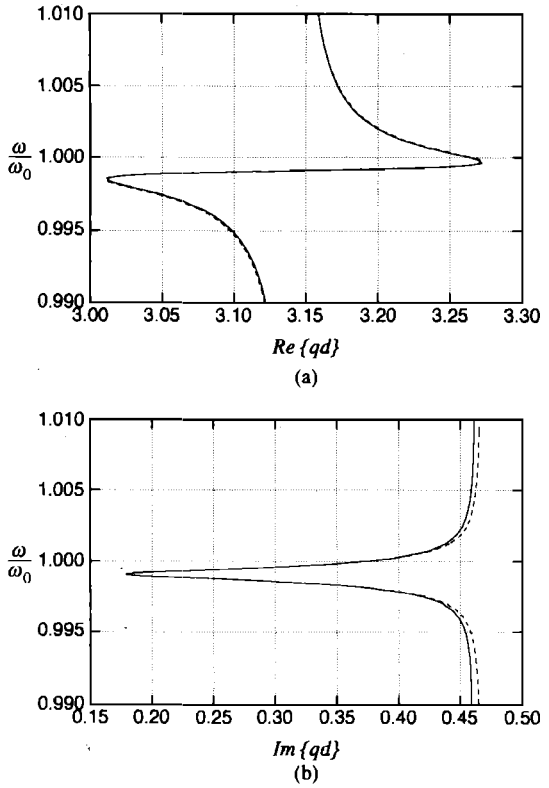

FIG. 8. Local structure of the stopping band in the lossy and degenerate case shown in Fig. 7. (a) and (b) show, respectively, the real and imaginary parts of qd as the abscissa and the normalized frequency ω/ω_0 as the ordinate where the solid lines represent the numerical solutions while the broken line represent the approximate solutions (50) and (51).

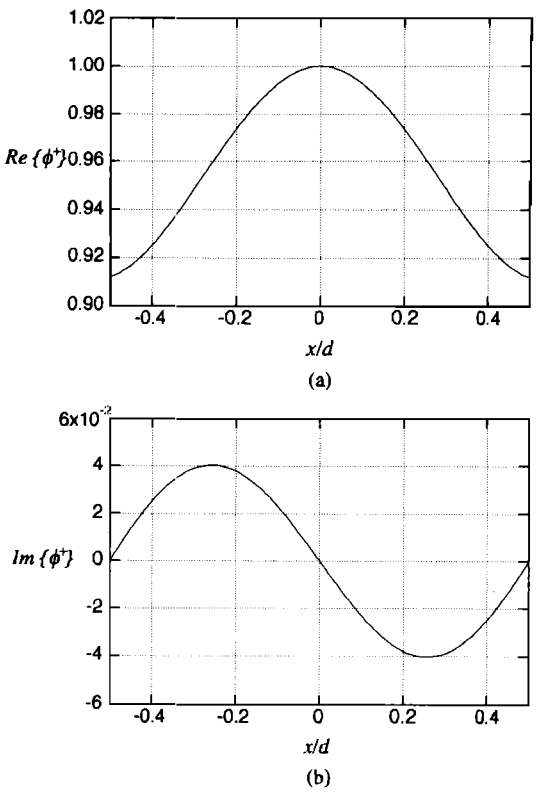

FIG. 9. Profile of the function $\phi^+(x)$ $[\equiv\Phi^+(x)/\Phi^+(0)]$ in the passing band ($\omega/\omega_0=3$); (a) and (b) show, respectively, its real and imaginary parts.

$$\frac{c_1^{\pm}}{c_2^{\pm}}=\frac{2}{\kappa\mathscr{Z}}\left[\pm\sin(qd)+\sin(kd)-\frac{\kappa\mathscr{Z}}{2}\cos(kd)\right]. \quad (57)$$

By these relations, it is found that c_2^+/c_1^+ is equal to c_1^-/c_2^- and that $\Phi^-(x)$ is derived from $\Phi^+(x)$, except a scale factor, only by reversal of the sign of x. If the approximate solution (22) is used in (56) and (57),[9] it follows that

$$\frac{c_2^+}{c_1^+}=\frac{c_1^-}{c_2^-}=\frac{\kappa\mathscr{Z}}{4\sin(kd)}+O(\kappa^2). \quad (58)$$

As is seen in (53), c_1^- and c_2^+ represent, respectively, the amplitudes of the reflected waves by the neighboring resonators. Since κ is small, the reflection is small of order κ in the passing bands. As $\mathscr{Z}$ tends to diverge or as $\sin(kd)$ tends to vanish, i.e., as a frequency approaches the stopping band, the relations (58) show that the reflection is enhanced.

In the stopping bands, however, (58) does not hold. If the lossless case is assumed, it can be shown, on setting $c_2^{\pm}/c_1^{\pm}=c^{\pm}\exp(i\alpha^{\pm})$, $c^{\pm}$ and $\alpha^{\pm}$ being real, that $|c^{\pm}|=1$ and

$$\tan\alpha^{\pm}=\frac{\pm i\sin(qd)}{\sin(kd)-(\kappa\mathscr{Z}/2)\cos(kd)}. \quad (59)$$

In the passing band, on the contrary, $c_2^{\pm}/c_1^{\pm}$ remains real as (56) and (57) suggest.

Figure 9 illustrates explicit profile of the function $\Phi^+(x)$ normalized by $\Phi^+(0)$ for a frequency in the passing band while Figs. 10 and 11 illustrate those for frequencies in the stopping bands due to the side branch resonance and due to the Bragg reflection with $m=1$. Assuming the dispersion relation in the lossless case shown in Fig. 2, ω/ω_0 is chosen in Figs. 9, 10, and 11, respectively, to be 3, 0.99, and 3.289. On setting $\Phi^+(x)/\Phi^+(0)$ to be $\phi^+(x)$, (a) and (b) in each figure show, respectively, the real and imaginary parts of $\phi^+(x)$. Since $\Phi^-(x)$ can be reproduced from $\Phi^+(x)$, its explicit profile is not given. Next, multiplying $\phi^+(x)$ by $\exp[i(qx-\omega t)]$ to derive the normalized Bloch wave function for the pressure disturbance in (55), Fig. 12 shows the resulting profile in the passing band with its real and imaginary parts in (a) and (b), respectively. It appears to be sinusoidal locally, but it is aperiodic. Figures 13 and 14 show the real part of the normalized Bloch wave function in the stopping band due to the side branch resonance and the Bragg reflection with $m=1$, respectively. Their imaginary parts can be proven to vanish identically because of the relation $c_2^+/c_1^+=\exp(i\alpha^+)$. But it is to be noted that the imaginary part of $\Phi^+(x)\exp(iqx)$, unless normalized, does not vanish and it decays as x increases in a similar fashion.

Here it should be remarked that the spatial profile of the Bloch wave function is discontinuous in slope at the connection points $x=(n+1/2)d$, although the magnitude of the jump is too small to be visible in Figs. 12 and 14. This can be understood as follows. For the time-harmonic disturbance, the pressure is proportional to the velocity potential if introduced. The boundary condition (15) for the continuity of pressure requires also the continuity of the velocity potential there. But the condition (14) implies that the spatial deriva-

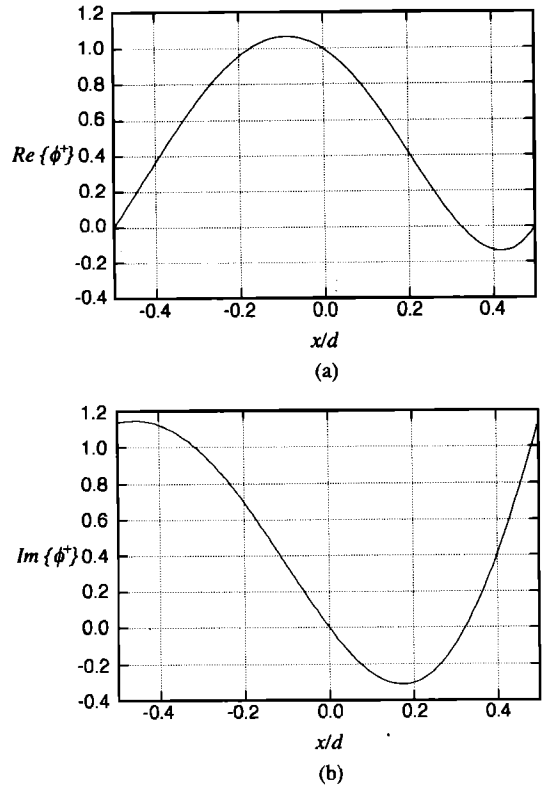

FIG. 10. Profile of the function $\phi^+(x)$ $[\equiv\Phi^+(x)/\Phi^+(0)]$ in the stopping band due to the side branch resonance ($\omega/\omega_0=0.99$); (a) and (b) show, respectively, its real and imaginary parts.

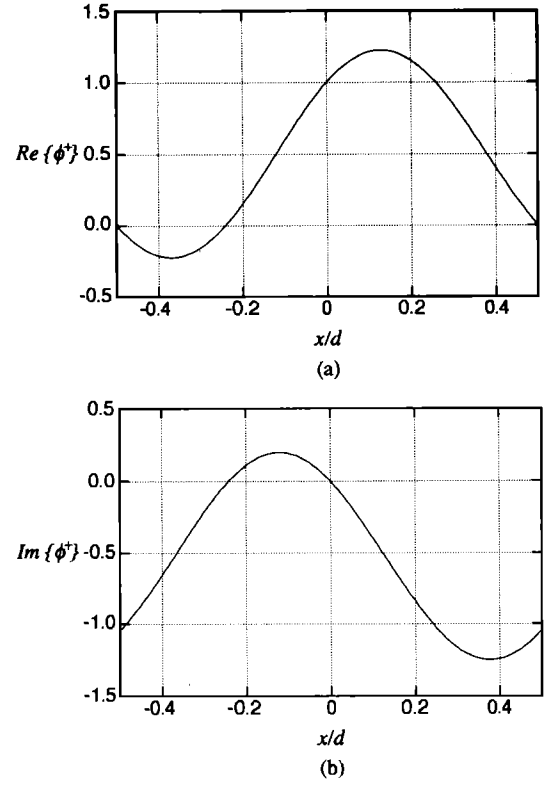

FIG. 11. Profile of the function $\phi^+(x)$ $[\equiv\Phi^+(x)/\Phi^+(0)]$ in the stopping band due to the Bragg reflection with $m=1$ ($\omega/\omega_0=3.289$); (a) and (b) show, respectively, its real and imaginary parts.

tives of the velocity potential are subjected to the jump to be balanced with the mass flux into the resonator.

IV. DISCUSSIONS ON CONTINUUM APPROXIMATION

In the light of the dispersion relation obtained, we now discuss the validity of the continuum approximation introduced in the previous paper.[1] This approximation exploits the assumption that a typical wavelength a_0/ω is much longer than the axial spacing d, i.e., $\omega d/a_0 \ll 1$ so that the array of resonators may be averaged per unit axial length of the tunnel. Then p' is governed by a following equation with the effect of the continuous distribution of the resonators on the right-hand side (see the Appendix):

$$\frac{\partial^2 p'}{\partial t^2} - a_0^2 \frac{\partial^2 p'}{\partial x^2} + \frac{2Ca_0^2\nu^{1/2}}{R^*} \frac{\partial^{-1/2}}{\partial t^{-1/2}} \left(\frac{\partial^2 p'}{\partial x^2} \right) - \nu_d \frac{\partial}{\partial t} \left(\frac{\partial^2 p'}{\partial x^2} \right) = -\kappa \frac{\partial^2 p_c'}{\partial t^2}, \tag{60}$$

where $1/R^* = (1 - BR/2Ad)/R$ and $R^* \approx R$ because $B \ll A$. This equation is closed by Eq. (10) with $p_t' = p'$. In a lossless case, these equations are combined into a following single equation:

$$\left[\left(\frac{\partial^2}{\partial t^2} + \omega_0^2 \right) \left(\frac{\partial^2}{\partial t^2} - a_0^2 \frac{\partial^2}{\partial x^2} \right) + \kappa\omega_0^2 \frac{\partial^2}{\partial t^2} \right] p' = 0. \tag{61}$$

Assuming p' and p_c' in the form of $\exp[i(lx - \omega t)]$, l being a wave number in the continuum approximation, the disper-

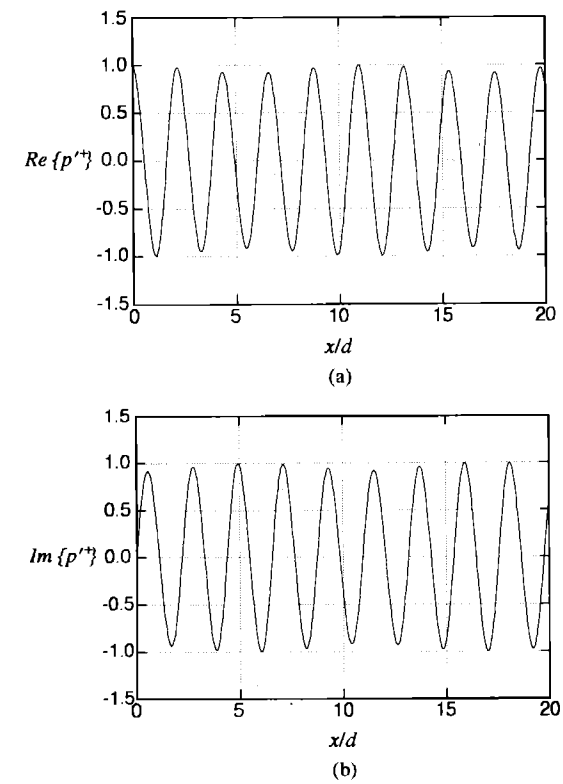

FIG. 12. Spatial profile of the normalized Bloch wave function for the pressure p'^+ $[\equiv\phi^+(x)\exp(iqx)]$ in the passing band ($\omega/\omega_0=3$); (a) and (b) show, respectively, its real and imaginary parts.

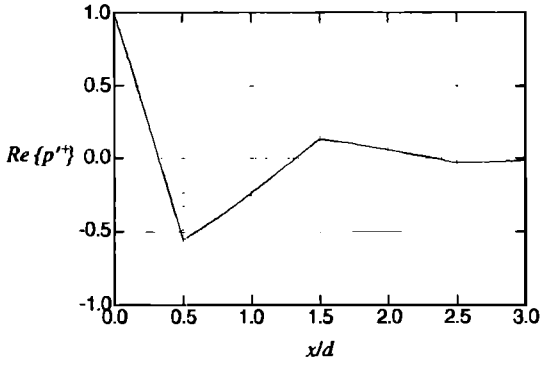

FIG. 13. Spatial profile of the normalized Bloch wave function for the pressure p'^{+} $[=\phi^{+}(x)\exp(iqx)]$ in the stopping band due to the side branch resonance ($\omega/\omega_0=0.99$) where only the real part is shown and the imaginary part vanishes identically.

sion relation of Eq. (60) with Eq. (10) is obtained as follows:

$$(ld)^2\left[1-\sqrt{2}(1+i)\frac{C}{R^*}\left(\frac{\nu}{\omega}\right)^{1/2}-\frac{i\nu_d\omega}{a_0^2}\right]=\left[1-\frac{\kappa}{Z_2(\omega)}\right]\psi^2, \tag{62}$$

where $Z_2(\omega)$ is defined by (21) and $\psi=\omega d/a_0(\ll 1)$.

We now examine the full dispersion relation (18) in a frequency domain corresponding to this approximation. In a lossless case, Eq. (18) is expanded in terms of $\omega d/a_0$ as

$$(qd)^2=(1+\kappa)\psi^2+\left(\frac{\kappa}{\psi_0^2}+\frac{\kappa^2}{12}\right)\psi^4+O(\psi^6), \tag{63}$$

with $\psi_0=\omega_0 d/a_0$ provided that ω is assumed to be much smaller than ω_0. But if ω_0 is assumed to be as small as ω, then the expansion should take the following form:

$$(qd)^2=\left[1-\frac{\kappa}{(\omega/\omega_0)^2-1}\right]\psi^2+O(\psi^4). \tag{64}$$

This dispersion relation agrees with (62) in the lossless case on identifying l to be q. In a low-frequency limit ($\omega\to 0$), the phase speed ω/l is found to be no longer a_0 but a slower value $a_0/(1+\kappa)^{1/2}$. As ω increases and the right-hand side

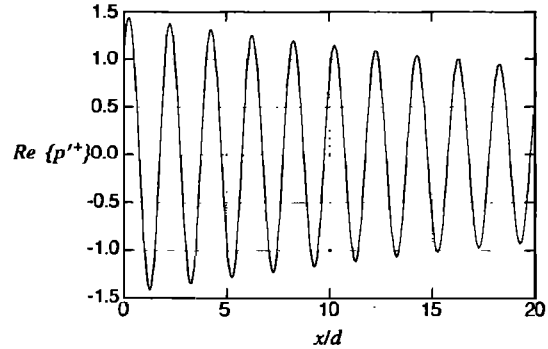

FIG. 14. Spatial profile of the normalized Bloch wave function for the pressure p'^{+} $[=\phi^{+}(x)\exp(iqx)]$ in the stopping band due to the Bragg reflection with $m=1$ ($\omega/\omega_0=3.289$) where only the real part is shown and the imaginary part vanishes identically.

of (64) becomes negative, the stopping band appears for $1<\omega/\omega_0<(1+\kappa)^{1/2}=1+\kappa/2+O(\kappa^2)$ but not below $\omega/\omega_0=1$. This result is consistent with (26) and (27), if the limit as $\psi_0\to 0$ is taken. In a lossy case, qd in (18) is expanded, on assuming ω_0 to be comparable with ω, into

$$(qd)^2=\left[1+\sqrt{2}(1+i)\frac{C}{R}\left(\frac{\nu}{\omega}\right)^{1/2}+\frac{i\nu_d\omega}{a_0^2}-\frac{\kappa}{Z_2(\omega)}\right]\psi^2, \tag{65}$$

where only the lowest dissipative terms are retained and the product of these terms with κ has been discarded because κ is also assumed small in the continuum approximation. It is readily seen that both dispersion relations (62) and (65) agree as far as the lowest dissipative terms are concerned and the difference $R-R^*$ is ignored.

Next, we discuss a far-field approximation introduced on top of the continuum approximation.[1] In the passing bands, both effects of the dissipation and of the resonators are negligibly small over a short distance such as several wavelengths. It is a far field that they manifest significantly due to their cumulative effects. To focus on this far field, we introduce a retarded time θ $(=t-x/a_0)$ measured by the sound speed a_0 instead of t but with the same spatial coordinate X $(=x)$. Suppose that both small effects due to the dissipation and the array of resonators were ignored completely, the sound waves are propagated with a_0 in the both directions of x. If only the wave propagating in the positive direction is pursued, then p' is given by a function of θ only and is independent of X. But when both effects are taken into account, p' now depends on X but *weakly*. Then a magnitude of $\partial p'/\partial X$ is much smaller than $a_0^{-1}\partial p'/\partial\theta$ by the order of δ, Re^{-1} or κ. Hence the first two terms on the left-hand side of Eq. (60) may be approximated as

$$\frac{\partial^2 p'}{\partial t^2}-a_0^2\frac{\partial^2 p'}{\partial x^2}=2a_0\frac{\partial^2 p'}{\partial X\,\partial\theta}-a_0^2\frac{\partial^2 p'}{\partial X^2}\approx 2a_0\frac{\partial^2 p'}{\partial X\,\partial\theta}. \tag{66}$$

Further neglecting the small derivative in X in the third and fourth terms of Eq. (60), we derive the evolution equation for p' in the far-field approximation as follows:

$$\frac{\partial p'}{\partial X}+\frac{C\nu^{1/2}}{a_0R^*}\frac{\partial^{1/2}p'}{\partial\theta^{1/2}}-\frac{\nu_d}{2a_0^3}\frac{\partial^2 p'}{\partial\theta^2}=-\frac{\kappa}{2a_0}\frac{\partial p_c'}{\partial\theta}, \tag{67}$$

where an integration constant depending on X has been set equal to zero by assuming a suitable condition. When the dispersion relation of Eqs. (67) with (10) is examined on assuming p' and p_c' in the form of $\exp[i(KX-\omega\theta)]$, K being a wave number in the far-field approximation, it follows that

$$Kd=\left[\frac{1+i}{\sqrt{2}}\frac{C}{R^*}\left(\frac{\nu}{\omega}\right)^{1/2}+\frac{i\nu_d\omega}{2a_0^2}-\frac{\kappa}{2Z_2(\omega)}\right]\psi. \tag{68}$$

From the definition of the phase $KX-\omega\theta=(K+\omega/a_0)x-\omega t$, $K+\omega/a_0$ corresponds to l so that Kd is nothing but $ld-\omega d/a_0$ $(=ld-\psi_0\omega/\omega_0)$. In fact, (68) is derived from (62) as far as the lowest dissipative effects are taken and $\kappa/Z_2(\omega)$ remains to be of order κ.

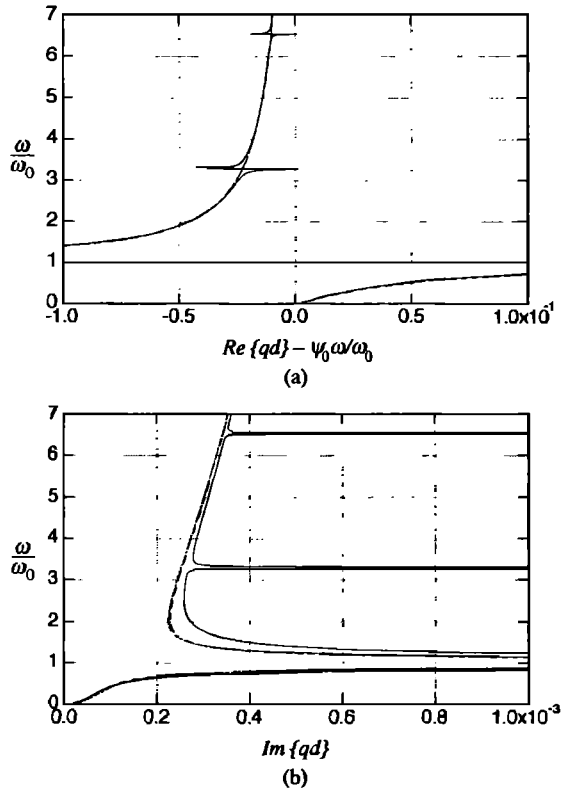

FIG. 15. Comparison of the dispersion relations by the continuum approximation and the far-field approximation with the full relation in the lossy case. (a) and (b) show, respectively, the real part of $qd-\psi_0\omega/\omega_0$ ($ld-\psi_0\omega/\omega_0$ or Kd) and the imaginary part of qd (ld or Kd) where the solid lines represent the full dispersion relation (18) while the dotted and broken lines represent the continuum approximation (62) and the far-field approximation (68), respectively.

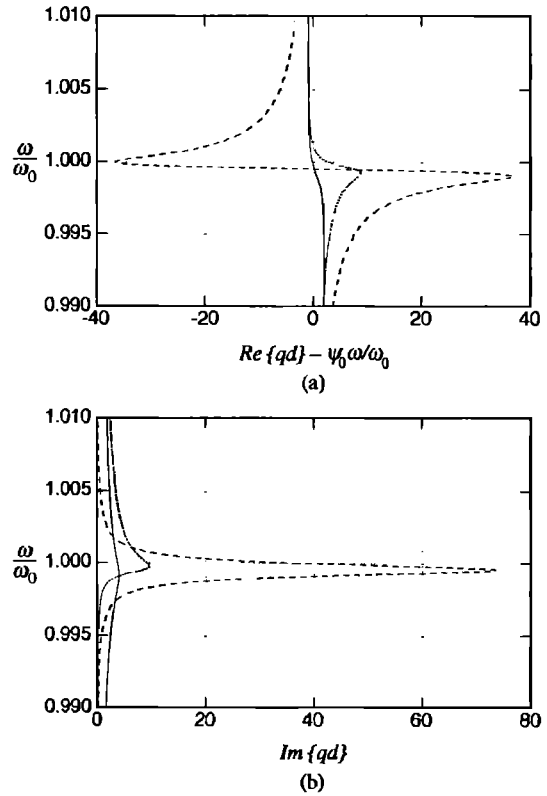

FIG. 16. Comparison of the local dispersion relations by the continuum approximation and the far-field approximation with the full relation in the lossy case. (a) and (b) show, respectively, the real part of $qd-\psi_0\omega/\omega_0$ ($ld-\psi_0\omega/\omega_0$ or Kd) and the imaginary part of qd (ld or Kd) where the solid lines represent the full dispersion relation (18) while the dotted and broken lines represent the continuum approximation (62) and the far-field approximation (68), respectively.

We now compare graphically the dispersion relations (62) and (68) by the continuum and far-field approximations with the full relation (18) in the lossy case. Figure 15(a) and (b) show, respectively, the real and imaginary parts of the wave number $qd-\psi_0\omega/\omega_0$ and the corresponding ones $ld-\psi_0\omega/\omega_0$ and Kd. The solid lines represent (18) while the dotted and broken lines represent (62) and (68), respectively. Except the Bragg reflections, they agree quantitatively and qualitatively as well beyond the low-frequency domain. But the imaginary part due to (18) is always greater than the remaining two, namely the continuum and far-field approximations underestimate the damping. Figure 16 magnifies Fig. 15 around the side branch resonance where the respective lines correspond to those used in Fig. 15. In a very narrow domain, three dispersion relations differ considerably. It is found that the continuum approximation, especially the far-field approximation overestimate both the dispersion and the damping in this domain.

V. CONCLUSIONS

The dispersion characteristics of sound waves in a tunnel with an array of Helmholtz resonators have been examined in detail over all frequency domain. It has been revealed that they exhibit the band structure by the side branch resonance and the Bragg reflections. Effect of the dissipation has been examined in detail and compared with the lossless case. In a plausible case, the wall friction and the diffusive effect of sound are very small except for the stopping bands. In a narrow frequency domain around the side branch resonance, the dissipative effects play a primary role to render the damping rate large but finite. For the Bragg reflection, however, the damping rates themselves are finite even in the lossless case so that the effects are found to remain secondary.

Interesting finding is that in case where the side branch resonance coincides with the Bragg reflection, the structure of the real and imaginary parts due to the side branch resonance is destroyed and the bandwidth is widened even in the lossless case. In the lossy case, however, it is found that the damping rate is suppressed significantly, though in the very narrow region around the frequency of the side branch resonance.

The continuum approximation and further the far-field approximation can provide a good description of the full dispersion relation in the low-frequency domain. Even beyond this domain, they agree well with the full dispersion relation, although they fail, of course, to describe the Bragg reflections resulting from the discrete distribution of the resonators. While both approximations underestimate the

damping over most of the frequency domain, it is noted that they overestimates the dispersion and the damping in a very narrow frequency domain around the side branch resonance.

ACKNOWLEDGMENT

The authors wish to thank Professor T. Kakutani for his comments on the manuscript.

APPENDIX

The Appendix is devoted to a brief derivation of the basic equation (3). In a framework of the linear theory, the equation of continuity and the equation of motion in the axial direction are given by taking account of both the wall friction due to the thin boundary layer and the diffusive effect of sound itself as follows:

$$\frac{\partial \rho}{\partial t}+\rho_0 \frac{\partial u}{\partial x}=\frac{1}{A}\oint \rho_0 v_n \, ds, \tag{A1}$$

$$\rho_0 \frac{\partial u}{\partial t}=-\frac{\partial p}{\partial x}+\left(\frac{4}{3}\mu+\mu_v\right)\frac{\partial^2 u}{\partial x^2}, \tag{A2}$$

where ρ, u, and p denote, respectively, the density, the axial velocity and the pressure, all averaged over the tunnel's cross section displaced by the boundary layer; v_n denotes the velocity component at the edge of the boundary layer directed normally inward of the cross section and the line integral is taken along its periphery, ds being the line element. At the edge of the boundary layer, v_n is related to u by the following fractional derivative of the minus half-order:[1,7]

$$v_n=C\nu^{1/2}\frac{\partial^{-1/2}}{\partial t^{-1/2}}\left(\frac{\partial u}{\partial x}\right). \tag{A3}$$

Thus the right-hand side of Eq. (A1) is given by $2\rho_0 v_n/R$ where R is a hydraulic radius of the cross section. In addition to (A1) and (A2), we require the equation of state for the ideal gas, which is given fully by

$$\frac{\rho}{\rho_0}=\left(\frac{p}{p_0}\right)^{1/\gamma}\exp\left(-\frac{S-S_0}{c_p}\right), \tag{A4}$$

where S denotes the entropy and the subscript 0 implies values at the equilibrium state.

Elimination of u and ρ from Eqs. (A1) to (A3) leads to Eq. (3) for $p'(=p-p_0)$. In this process, the small entropy change due to the thermoviscous effect[1,7]

$$S-S_0=-\frac{(\gamma-1)k_T}{\gamma p_0}\frac{\partial u}{\partial x}, \tag{A5}$$

must be included through

$$\frac{\partial \rho}{\partial t}=\left.\frac{\partial \rho}{\partial p}\right|_S \frac{\partial p}{\partial t}+\left.\frac{\partial \rho}{\partial S}\right|_p \frac{\partial S}{\partial t}. \tag{A6}$$

Since only the lowest dissipative effects are concerned here, the lowest relations in the equations

$$\frac{\partial^2 u}{\partial x^2}=\frac{1}{a_0^2}\frac{\partial^2 u}{\partial t^2}=-\frac{1}{\rho_0 a_0^2}\frac{\partial^2 p}{\partial x\,\partial t} \tag{A7}$$

are used to evaluate the dissipative terms to yield Eq. (3). Therefore $\partial^2 p/\partial x^2$ in the third and fourth terms of Eq. (3) may be replaced by $a_0^{-2}\,\partial^2 p/\partial t^2$. Both equations are asymptotically equivalent, though mathematically different equations, of course. In view of the number of initial and boundary conditions to be imposed, however, the alternative equation is inappropriate.

Finally we mention the derivation of Eq. (60) by the continuum approximation for the array of resonators. Comparing with the derivation above, only difference lies in evaluation of the right-hand side of Eq. (A1). When the resonators are connected, the integration of the velocity v_n along the periphery is divided into two parts, one being due to the boundary layer on the tunnel wall and the other due to the resonator. Denoting the velocity (A3) at the edge of the boundary layer by v_b and the velocity into the resonator by $-w$, respectively, the right-hand side of (A1) is evaluated per unit axial length of the tunnel as[1]

$$\frac{1}{A}\oint \rho_0 v_n \, ds=\frac{1}{A}\left[\left(\frac{2A}{R}-NB\right)\rho_0 v_b-NB\rho_0 w\right], \tag{A8}$$

where N $(=1/d)$ is the number density of the resonators along the tunnel. By using (A3) and $B\rho_0 w=(V/a_0^2)\partial p_c'/\partial t$ derived from (7) with $w_c=w$ and the adiabatic approximation, (A8) is written as

$$\frac{2\rho_0 C\nu^{1/2}}{R^*}\frac{\partial^{-1/2}}{\partial t^{-1/2}}\left(\frac{\partial u}{\partial x}\right)-\frac{\kappa}{a_0^2}\frac{\partial p_c'}{\partial t}, \tag{A9}$$

where $1/R^*$ is defined as $(1-BR/2Ad)/R$ and $R\approx R^*$ because $B/A=(r/R)^2\ll 1$ and $\kappa=V/Ad$. Following the same procedure leading to Eq. (3), we arrive at Eq. (60) which takes account of the array of resonators based on the continuum approximation.

[1] N. Sugimoto, "Propagation of nonlinear acoustic waves in a tunnel with an array of Helmholtz resonators," J. Fluid Mech. **244**, 55–78 (1992).

[2] N. Sugimoto, "'Shock-free tunnel' for future high-speed trains," in *Proceedings of International Conference on Speed-Up Technology for Railway and Maglev Vehicles*, edited by M. Iguchi (Japan Society of Mechanical Engineers, Tokyo, 1993), Vol. 2, pp. 284–292.

[3] L. Brillouin, *Wave Propagation in Periodic Structures* (Dover, New York, 1953).

[4] C. Kittel, *Introduction to Solid State Physics* (Wiley, New York, 1976), 5th ed.

[5] C. E. Bradley, "Acoustic Bloch wave propagation in a periodic waveguide," Technical Report of Applied Research Laboratories, ARL-TR-91-19 (July), The University of Texas at Austin (1991).

[6] For an harmonic wave of 5 Hz to be decayed to be half in amplitude by the action of the wall friction, it takes a propagation distance of about 50 km in a tunnel of diameter 10 m. If the decay is achieved only by the action of the diffusivity of sound itself, it takes one and half million kilometers!

[7] N. Sugimoto, "Generalized Burgers equations and fractional calculus," in *Nonlinear Wave Motion*, edited by A. Jeffrey (Longman, London, 1989), pp. 162–179.

[8] This can be seen by inserting (22) into (18) and expanding it in terms of κ if $\sin(kd)$ were assumed to be much smaller than κ and $\cos(\frac{1}{2}\kappa\mathscr{Z})$ must be taken up to $O(\kappa^2)$. In fact, the expansion (22) exhibits the nonuniformity in the coefficient of κ^2 as $qd=kd-\kappa\mathscr{Z}/2-\kappa^2\mathscr{Z}^2\cot(kd)/8+O(\kappa^3)$.

[9] In order to obtain c_2^+/c^+ by using (56), for example, (22) is required to be specified up to $O(\kappa^2)$ inclusive (see Ref. 8).